catalysts

MDPI

Article

Sb-Containing Metal Oxide Catalysts for the Selective Catalytic Reduction of NO_x with NH_3

Qian Xu [1], Dandan Liu [1], Chuchu Wang [1], Wangcheng Zhan [1], Yanglong Guo [1], Yun Guo [1], Li Wang [1,*], Qingping Ke [2] and Minh Ngoc Ha [3]

1 Key Laboratory for Advanced Materials and Research Institute of Industrial Catalysis, School of Chemistry & Molecular Engineering, East China University of Science and Technology, 130 Meilong Road, Shanghai 200237, China; Y11140023@mail.ecust.edu.cn (Q.X.); Y30181049@mail.ecust.edu.cn (D.L.); wangyongchuchu@163.com (C.W.); zhanwc@ecust.edu.cn (W.Z.); ylguo@ecust.edu.cn (Y.G.); yunguo@ecust.edu.cn (Y.G.)

2 College of Chemistry and Chemical Engineering, Anhui University of Technology, Maanshan 243002, China; Qingke@ahut.edu.cn

3 VNU Key Laboratory of Advanced Material for Green Growth, VNU University of Science, Vietnam National University, Hanoi 100000, Vietnam; haminhngoc@hus.edu.vn

* Correspondence: wangli@ecust.edu.cn

Received: 30 August 2020; Accepted: 30 September 2020; Published: 8 October 2020

check for updates

Abstract: Sb-containing catalysts ($SbZrO_x$ (SbZr), $SbCeO_x$ (SbCe), $SbCeZrO_x$ (SbCeZr)) were prepared by citric acid method and investigated for the selective catalytic reduction (SCR) of NO_x with NH_3 (NH_3-SCR). SbCeZr outperformed SbZr and SbCe and exhibited the highest activity with 80% NO conversion in the temperature window of 202–422 °C. Meanwhile, it also had good thermal stability and resistance against H_2O and SO_2. Various characterization methods, such as XRD, XPS, H_2-TPR, NH_3-TPD, and in situ diffuse reflectance infrared Fourier transform (DRIFT), were applied to understand their different behavior in NO_x removal. The presence of Sb in the metal oxides led to the difference in acid distribution and redox property, which closely related with the NH_3 adsorption and NO oxidation. Brønsted acid and Lewis acid were evenly distributed on SbCe, while Brønsted acid dominated on SbCeZr. Compared with Brønsted acid, Lewis acid was slightly active in NH_3-SCR. The competition between NH_3 adsorption and NO oxidation was dependent on SbO_x and metal oxides, which were found on SbCe while not on SbCeZr.

Keywords: SbCeZr; NH_3-SCR; active sites; mechanism

1. Introduction

Nitrogen oxide (NO_x), one of the main environmental contaminants emitted from stationary sources and mobile sources, causes photochemical smog, acid rain, and the depletion of the ozone layer [1,2]. Several technologies have been proposed for NO_x removal, such as direct decomposition of NO_x, NO_x storage reduction (NSR), and the selective catalytic reduction (SCR) process with ammonia (NH_3-SCR) or hydrocarbons (HC-SCR). The NH_3-SCR process has been proven to be the efficient method to satisfy the restrict regulations of NO_x emissions [3]. In general, the NH_3-SCR reaction is a competitive process between NH_3 oxidation and NO_x reduction, which are closely affected by reaction temperature. The enhanced oxidation activity at low temperature promotes NO_x selective reduction, while it also takes a risk for the depletion of NH_3 at high temperature leading to the decrease in NO reduction. Meanwhile, the reaction thermal shock and exhaust components (H_2O and SO_2) put forward strict requirements on the design of NH_3-SCR catalysts.

CeO_2 possesses unique oxygen storage-release capability by the formation of Ce^{3+}/Ce^{4+} redox couples [4], but the maximum NO conversion on CeO_2 was about 30% in the whole temperature

range. Compared with mono-metal oxides, dual metal oxides have been more active in NO abatement. The presence of Ti, W, Mo, Mn, and Nb can efficiently broaden the temperature window, especially the introduction of W. Nearly 100% NO_x conversion could be achieved on $CeWO_x$ in a wide temperature range (250–425 °C) under a rather high gas hourly space velocity (GHSV) (500,000 h^{-1}). The effects of SO_2 on the SCR over CeO_2 was strongly dependent on the SO_2 content and reaction conditions. An appropriate level for sulfated pretreatment can promote SCR, and the presence of excess SO_2 shows obvious negative effects. Li studied that SO_2 was preferentially bonded with CeO_2 as sulfate species leading to a significant decrease in reducibility and the loss of surface active oxygen groups [5]. Suitable sulfation promoted NH_3 adsorption and favored the formation of oxygen vacancies which facilitated NH_3-SCR [6]. Hong's research indicated that the optimal condition for sulfation treatment was 800 ppm SO_2 1 h at 500 °C [7]. Meanwhile, the thermal stability of the sulfated Ce-based catalyst needs to be further improved [8].

Sb compounds are generally classified into the valences of +3 and +5, in which the oxidation state of +5 is more stable. The Sb-containing oxides are Sb_2O_3, Sb_2O_5, and mixed oxide Sb_2O_4 that is composed of Sb^{3+} and Sb^{5+} [9]. Sb has been widely used as a promoter for NH_3-SCR catalysts [6,7]. The surface acid and the redox capability are generally considered to be two necessary factors for NH_3-SCR catalysts [10–12]. The addition of Sb can improve the dispersion of active species [13] and increase acid sites and the redox property [14], which are due to the strong interaction between SbO_x and other metal oxides [15,16]. Besides the promotion in activity, the resistance of K_2O poisoning [17] and SO_2 are also found [18] in Sb-containing catalysts. The role of Sb as a promoter reflects in minimizing the binding affinity between the catalytic surface and the ammonium (bi)sulfates species, which is beneficial for the low-temperature SO_2 resistance [19].

The substitution of Ce^{4+} by Zr^{4+} helps create structural defect, accelerating oxygen diffusion and the formation of surface oxygen species [20], which can consequently promote the redox property [21,22]. $CeZrO_x$ mixed oxide with remarkable thermal stability shows an enormous advantage in NH_3-SCR [23,24]. In this study, Sb-containing metal oxides (SbZr, SbCe, SbCeZr) were prepared by citric acid method and investigated for NO_x removal by NH_3-SCR. The SbCeZr exhibited higher catalytic activity than SbCe and SbZr catalysts, especially in the presence of H_2O and SO_2. The correlation between physicochemical properties and SCR performance was explored by various characterization techniques, and the mechanism was also studied using in situ diffuse reflectance infrared Fourier transform spectroscopy (DRIFT).

2. Results and Discussion

2.1. Catalyst Activity

2.1.1. NH_3-SCR Performance

NO_x conversions over the catalysts as a function of temperature are illustrated in Figure 1a. Pristine SbO_x and SbZr showed negligible catalytic activity with NO_x conversion below 10% in the whole temperature range. Even for CeO_2, the maximum NO_x conversion was only 29% at 360 °C. The addition of Sb promoted the NO_x conversion over Ce-containing catalysts, and SbCeZr exhibited better NH_3-SCR performance than SbCe. The temperature for 50% conversion (T_{50}) was 175 °C over SbCeZr, which was lower than that of SbCe (223 °C). The operation temperature window (NO_x conversion over 80%) was 202–422 °C over SbCeZr, while it was 261–407 °C over SbCe.

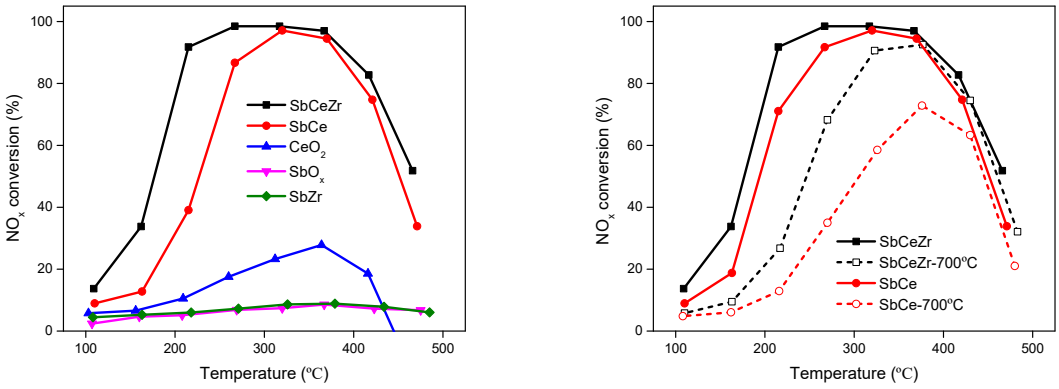

(**a**) (**b**)

Figure 1. (**a**) NO_x conversions and (**b**) thermal stability over the catalysts (reaction conditions: 500 ppm NO, 500 ppm NH_3, 5% O_2, with Ar balance).

The apparent activation energy of the NH_3-SCR reaction is an important factor to evaluate the role and efficiency of the catalyst in the reaction [25]. By calculating the reaction rate constant of the NH_3-SCR reaction over SbCeZr and SbCe, the apparent activation energy of the catalysts were obtained. The reaction activation energy over the SbCeZr catalyst (33.3 kJ/mol) was lower than that of the SbCe catalyst (42.1 kJ/mol), which further confirmed the excellent NH_3-SCR reaction performance of SbCeZr.

In order to investigate the thermal stability of SbCeZr and SbCe, the catalysts were aged at 700 °C for 4 h in the air before testing. As shown in Figure 1b, aging had a side effect on catalytic activity, which led to the loss in activity and shrink from the operation temperature window. The presence of Zr improved the thermal resistance of thermal shock. T_{50} of aged SbCeZr turned out to be 247 °C and the operation temperature window narrowed to 300–413 °C, resulting from the sintering. The maximum NO_x conversion over aged SbCe was only 73% at 373 °C, i.e., aging led to the significant deactivation.

2.1.2. Effects of H_2O and SO_2

SO_2 and H_2O are unavoidable in the feed gas, so the effect on the catalytic activities over SbCeZr and SbCe were investigated. As shown in Figure 2a, the NH_3-SCR performance of SbCeZr was slightly affected by SO_2 or H_2O at temperatures below 220 °C. However, the presence of H_2O significantly reduced the catalytic activity at temperatures above 420 °C, which could be attributed to the competitive adsorption between H_2O and NH_3 [26,27]. In the presence of O_2 and SO_2, the deposited sulfates on the catalysts led to the decrease of the specific surface area (SSA) [28] and blocked the active sites at low temperature [29]. With increased temperature, the decomposition of sulfates led to the restoration of active sites [30]. The presence of H_2O facilitated SO_2 oxidation at low temperature and inhibited sulfate decomposition at high temperature. Therefore, the presence of H_2O and SO_2 had a more detrimental effect than H_2O or SO_2.

The presence of SO_2 on SbCe had an influence similar to that on SbCeZr. Unfortunately, the presence of H_2O had a detrimental effect on NH_3-SCR performance over SbCe. The light-off temperature (T_{50}) shifted to 284 °C, and the maximum NO_x conversion was only 66% at 370 °C. When both H_2O and SO_2 were introduced simultaneously, the synergy effect made the NH_3-SCR performance drop even more. T_{50} shifted to high temperature and the maximum NO_x conversion also decreased accordingly. The decrease of NH_3-SCR performance was not only related to the formation of ammonium salt on the catalyst surface but also connected with the fact that the active phase was sulfated and then formed stable sulfate species [31].

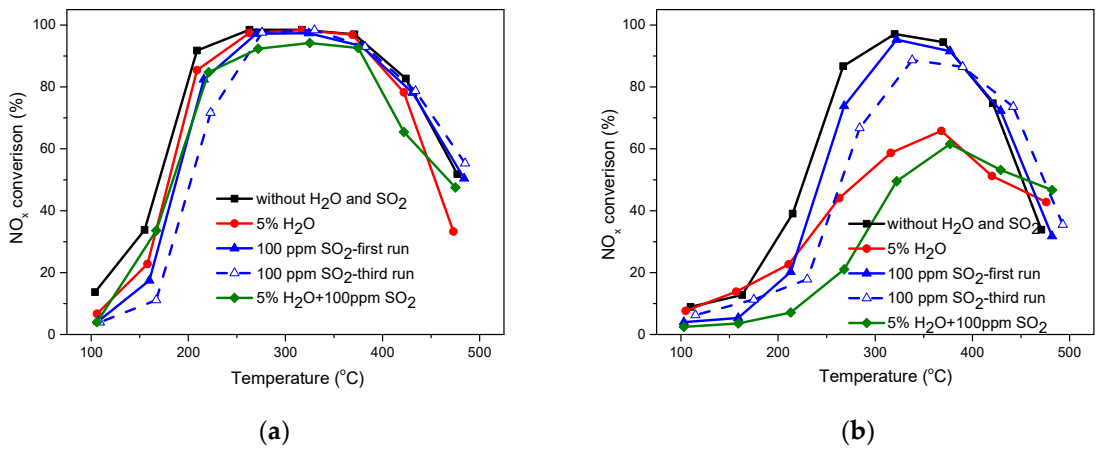

Figure 2. Effect of H_2O and SO_2 on the NH_3-SCR performance over (**a**) the SbCeZr catalyst and (**b**) the SbCe catalyst (reaction conditions: 500 ppm NO, 500 ppm NH_3, 5% O_2, 5% H_2O, 100 ppm SO_2, with Ar balance).

Furthermore, repeated temperature ramps (three times) containing SO_2 over the SbCeZr catalyst and the SbCe catalyst were also conducted. For SbCeZr, the second time was consistent with the third time, and slightly less active than the first time below 250 °C. It suggests that SbCeZr had a better performance of resistance to SO_2. For SbCe, during the three test ramps, the T_{80} kept shifting to higher temperatures, which narrowed the operation window.

2.2. Catalyst Characterization

2.2.1. XRD

The XRD patterns of the fresh and aging catalysts are shown in Figure 3. The XRD patterns of CeO_2 and ZrO_2 showed sharp diffraction peaks corresponding to CeO_2 with a cubic fluorite structure (JCPDS 34-0394, 2θ = 28.6°, 47.5°, and 56.4°) and tetrahedral ZrO_2 (JCPDS 50-1089, 2θ = 30.1°, 50.4°, and 60.0°). The typical peaks at 19.8°, 25.7°, and 29.0° over SbO_x were observed and assigned to Sb_2O_4 (JCPDS 11-0694). Compared with the XRD pattern of CeO_2, the diffraction peaks of CeZr shifted to high angles, suggesting that Zr was incorporated into the CeO_2 crystal lattice to form a $CeZrO_4$ solid solution.

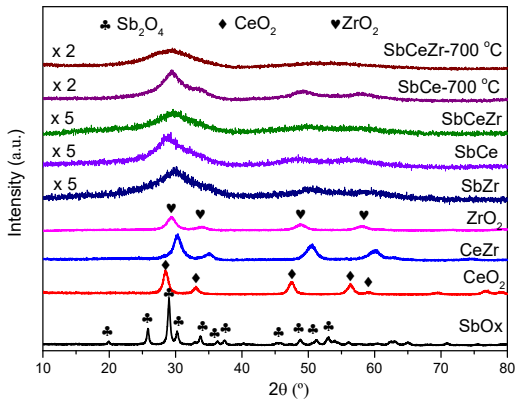

Figure 3. XRD patterns of the catalysts.

With the introduction of Sb, the diffraction peaks were broadened and weakened, which led to the absence of obvious peaks. No diffraction peaks related to SbO_x were detected, and a completely amorphous structure was formed on the Sb-containing catalysts. Compared with the fresh samples,

the diffraction peaks of aged catalysts (aging at 700 °C in air for 4 h) intensified, indicating the increase in the grain size.

According to Table 1, the specific surface area (SSA) of SbCeZr (73 m^2/g) was slightly higher than that of SbCe (68 m^2/g). Combining the value of specific surface area (Table 1) with activity showed that specific surface area was not the decisive factor in catalyst activity. It thus suggested that other factors were affecting activity. The loss of SSA was found after aging, especially on SbCe. The SSA of SbCe-700 °C was only 9 m^2/g, which was only 13% of fresh SbCe. However, 57% SSA of SbCeZr was lost after aging. Combining the results of XRD and SSA showed that SbCeZr possessed the higher thermal stability as compared to SbCe.

Table 1. Brunauer–Emmett–Teller (BET) specific surface area (SSA), bulk phase, and surface atom concentration of the catalysts.

Sample	S_{BET} (m^2/g) [a]	Sb/(Ce+Zr) [b]	Surface Atom Concentration (%) [c]			
			Sb/(Ce + Zr)	Sb^{5+}/Sb	Ce^{3+}/Ce	$O_\alpha/(O_\alpha + O_\beta)$
SbO_x	-	-	-	50.3	-	38.1
SbZr	32	0.68	1.09	55.3	-	33.4
SbCe	68	1.02	1.59	62.2	32.9	40.6
SbCeZr	73	0.57	0.66	64.3	42.1	47.8

[a] Specific surface area determined by N_2 adsorption-desorption. [b] Sb/(Ce+Zr) mole ratio detected by ICP-AES. [c] Surface atom concentration detected by XPS analysis.

2.2.2. XPS

Figure 4 presented the XPS spectra of Sb 3d, Ce 3d, and O 1s for Sb-containing catalysts, and the surface atom concentration and chemical state are summarized in Table 1. For the SbCeZr catalyst, the bulk phase mole ratio of Sb/(Ce + Zr) was 0.57, slightly lower than the surface atom concentration ratio 0.66. However, as for the SbCe catalyst and SbZr catalyst, the bulk phase mole ratio was much lower than the surface concentration. These results indicated that more Sb existed on the surface of CeO_2 and ZrO_2 over SbCe and SbZr, while more Sb was incorporated into the $CeZrO_x$.

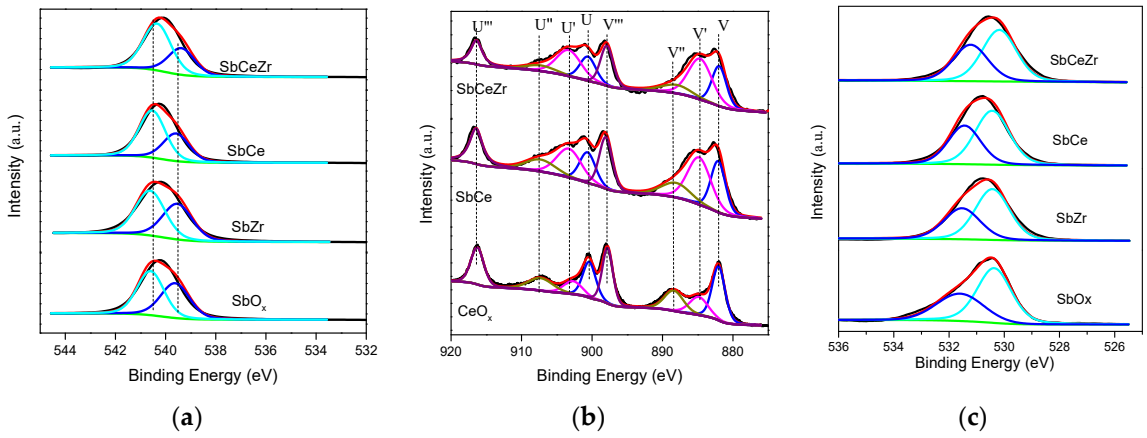

Figure 4. XPS spectra for (**a**) Sb3d, (**b**) Ce3d, and (**c**) O1s over the catalysts.

Figure 4a showed the Sb $3d_{3/2}$ spectra of Sb-containing catalysts and SbO_x. Because of the O 1s and Sb $3d_{5/2}$ photoemission line overlapping around 530.0 eV, the Sb$3d_{3/2}$ spectra at higher binding energy were used. This peak could be separated into two contributions—the Gaussian line centered at 540.4 eV corresponds to antimony with an oxidation state of Sb^{5+}, while the peak at 539.6 eV corresponds to Sb^{3+} [9,16,32]. As shown in Table 1, the proportion of Sb^{5+} increase followed the order of SbO_x < SbZr < SbCe < SbCeZr. The ratio of Sb^{5+} over SbO_x was 50.3%, meaning an equal proportion of Sb^{5+} and

Sb^{3+}, i.e., Sb_2O_4 was the main species in SbO_x, which was in line with the XRD results. It was obvious that the concentration of Sb^{5+} over the SbCeZr was significantly improved to 64.3%.

Figure 4b presents the Ce 3d spectra of the catalysts. The Ce 3d peaks could be deconvoluted into four pairs of spin-orbit doublets. Four main peaks in $3d_{5/2}$ at 881.9, 884.9, 887.8, and 898.0 eV were labeled as V, V′, V″, and V‴, respectively. The four main peaks in $3d_{3/2}$ at 900.8, 903.0, 907.4, and 916.2 eV were labeled as U, U′, U″, and U‴, respectively. The peaks labeled as V′ and U′ corresponded to Ce^{3+} and the other peaks labeled as V, V″, V‴, U, U″, and U‴ corresponded to Ce^{4+} [12,33]. From the Ce 3d XPS spectra, it could be concluded that the Ce^{3+} and Ce^{4+} species coexisted in all the samples, and the ratios of $Ce^{3+}/(Ce^{4+} + Ce^{3+})$ of all the catalysts are listed in Table 1. The $Ce^{3+}/(Ce^{4+} + Ce^{3+})$ ratio over SbCeZr (42.1%) was higher than that over SbCe (32.9%). The presence of Sb^{5+} led to the increase of the Ce^{3+} concentration due to the redox reaction $Sb^{3+} + Ce^{4+} \leftrightarrow Sb^{5+} + Ce^{3+}$. The transformation of Ce^{4+} to Ce^{3+} created the charge imbalance and oxygen vacancy, facilitating the adsorption of oxygen species or activation of reactants in NH_3-SCR [34].

The O 1s spectra of all the catalysts are displayed in Figure 4c. The spectra were deconvoluted into two peaks. The peak at 530.2 eV was attributed to lattice oxygen (O_β), and the other one at around 531.2 eV was denoted to surface chemisorbed oxygen (O_α). O_α species usually correlated with oxygen defects or surface oxygen, such as O_2^{2-} or O_2^{-} [35–37]. The relative ratios of $O_\alpha/(O_\alpha + O_\beta)$ by peak deconvolution over the samples were 47.8%, 40.6%, and 33.4% over SbCeZr, SbCe, and SbZr, respectively, suggesting more surface chemisorbed oxygen formed over SbCeZr.

2.2.3. H_2-TPR

The redox property of catalysts plays an important role in the NH_3-SCR reaction [37,38]. Figure 5 shows the H_2-TPR profiles of the catalysts. CeO_2 showed two reduction peaks centered at 474 and 781 °C, which were attributed to the reduction of surface oxygen and bulk oxygen of CeO_2, respectively [22,39]. SbO_x also showed two reduction peaks centered at 616 and 701 °C, which could be ascribed to the reduction of Sb^{5+} to Sb^{3+} and Sb^{3+} to Sb^0, respectively [9]. The reduction profiles of SbZr were similar to those of SbO_x with the reduction temperature shifting to lower temperature.

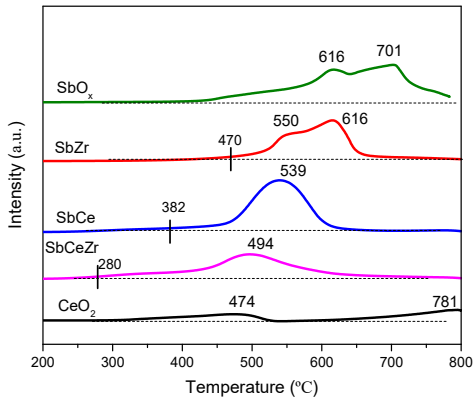

Figure 5. H_2-TPR profiles of the catalysts.

The reduction behavior of SbCe and SbCeZr was different from that of CeO_2 and SbO_x. A broad peak was observed on SbCe and SbCeZr centered at 539 °C and 494 °C, respectively, which could be attributed to the combination of reduction peaks of SbO_x and CeO_2 [40]. The broad reduction peak of SbCeZr shifted to lower T_{onset} (the onset reduction temperature of active oxygen) compared to the other catalysts (SbCe and SbZr). The lower reduction temperature of SbCeZr indicated the increase in redox and the generation of easily reducible species.

H_2-TPR is usually used as a descriptor for the relative strength of the interaction among active components. The similar reduction profiles of SbO_x and SbZr suggested the rather weak interaction between SbO_x and ZrO_2. However, a strong interaction was found on SbCe due to the co-reduction of

SbO_x and CeO_2, which also led to the higher reduction temperature. By contrast, with the help of ZrO_2, the strong interaction between SbO_x and CeO_2 was weakened, resulting in the lower onset reduction temperature of active oxygen.

2.2.4. NO-TPD

NO-TPD experiments were performed to investigate the adsorption and oxidation properties of NO_x on different catalysts. NO-TPD profiles and the calculated NO_x adsorption capacity are presented in Figure 6 and Table 2, respectively. The NO desorption peak below 100 °C was attributed to physical adsorbed NO, and the one at about 260 °C was attributed to chemical adsorbed NO [34]. Since the strength of NO bonding to the ceria surface depends on the reduction degree of support (unsaturated sites) [41], it could be concluded that the Ce^{3+} content on the SbCeZr surface was much higher than that of SbCe, which was consistent with the XPS result.

Table 2. H_2 consumption, NH_3 desorption amount, and strong acid and NO_x adsorption capability of the catalysts.

Sample	H_2 Consumption [a] (mmol/g)	NH_3-TPD Result [b]			NO_x Adsorption Capability [c] (μmol/g)	
		Acid Amount (mL/g)	B/(A + B + C + D)	(C + D)/(A + B + C + D)	NO_x	NO_2
SbZr	5.17	0.78	0.38	0.27	138.7	15.8
SbCe	4.30	0.95	0.34	0.30	63.5	8.6
SbCeZr	3.81	1.46	0.40	0.29	147.7	46.7

[a] The amount of H_2 consumption quantified by CuO as a calibration reference. [b] Acid amount and acid ratio calculated by NH_3 desorption peak area in NH_3-TPD. [c] NO_x adsorption capability calculated from NO-TPD.

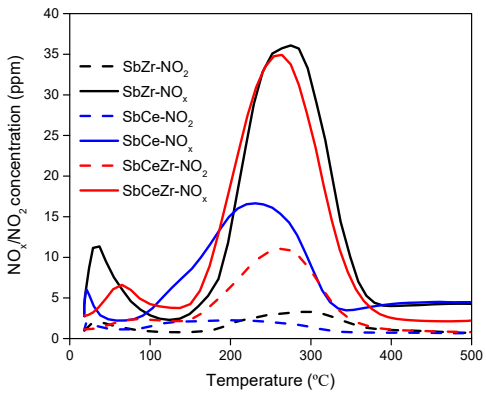

Figure 6. NO-TPD profiles of the catalysts.

NO_2 came from the oxidation of adsorbed NO by active oxygen on the catalyst surface. The desorption temperature and peak area correlated with the adsorption strength and oxidation ability of NO. The ability of the catalyst for oxidizing NO to NO_2 plays an important role in improving the catalytic activities since it can promote the occurrence of the "fast SCR" reaction [42,43]. Considering the temperature range of the NH_3-SCR reaction, the desorbed peaks in the temperature range of 150–400 °C were mainly discussed.

The main NO_x desorption peak of SbCe was at 245 °C, slightly lower than those of SbCeZr (258 °C) and SbZr (273 °C). The calculated NO_x amount was in the order of the following sequence: SbCeZr > SbZr > SbCe. There were no obvious differences in the NO_x desorption amount between SbCeZr and SbZr, but the amount of NO_x desorption on SbCeZr was almost 2 times higher than that of SbCe. It is worth mentioning that 31.7% NO converted to NO_2 on SbCeZr, while only 13.5% NO did so on SbCe. With the help of NO_2, the "fast SCR" occurred and facilitated NO_x removal.

2.2.5. NH_3-TPD

Surface acidity of the catalysts plays a key role in the adsorption and activation of NH_3 [44,45]. NH_3-TPD experiments were conducted to characterize the acid amount and strength according to peak area and desorption temperature, and the profiles are shown in Figure 7. Four broad peaks could be observed in the NH_3-TPD profiles in the temperature range of 100–450 °C. NH_3 desorption peaks at low temperature (<200 °C) were associated with NH_3 desorption from weak acid sites derived from coordinatively unsaturated Ce^{n+} or Zr^{n+} sites [46,47], and the peaks in the temperature range of 200–300 °C were assigned to the dissociation of NH_4^+ on Brønsted acid sites associated with surface hydroxyl groups. The peaks at temperatures higher than 300 °C were denoted as NH_3 desorption from strong Lewis acid [48–50]. The original weak Lewis acidity of CeO_2 and ZrO_2 was also increased by SbO_x loading, which could be attributed to the electron withdrawing of SbO_x species in proximity of Ce^{n+}/Zr^{n+} Lewis acid sites. The NH_3 species desorbed from acid sites (>200 °C) played a decisive role in the NH_3-SCR reaction [51,52].

The nature of the active sites could be assessed based on the quantity of sites and their intrinsic activity [49]. Quantitative analysis was employed to compare the amount of acid sites, and the ratios of different species based on the deconvoluted results are also shown in Table 2. The amount of acid sites had the following sequence: SbCeZr > SbCe > SbZr. The large total acid amount was found over SbCeZr (1.46 mL/g), which was nearly 2 times as much as that on SbZr (0.78 mL/g). It suggested that the interaction among the catalyst components facilitated the increase in acid amount.

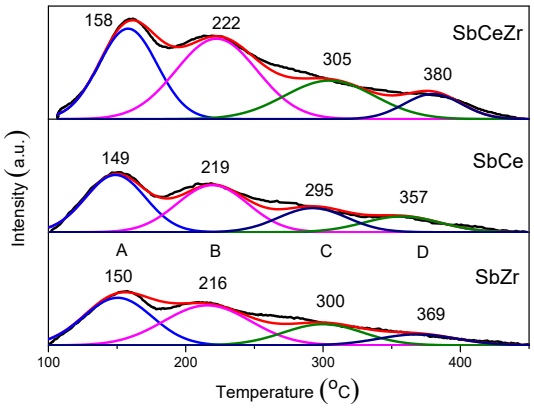

Figure 7. NH_3-TPD profiles of the catalysts.

2.3. In Situ DRIFT

2.3.1. Adsorption of NH_3

The adsorption and activation of NH_3 play an important role in the NH_3-SCR reaction [53]. The adsorption of NH_3 was investigated by in situ DRIFT shown in Figure 8. The bands at 3166, 3241, and 3357 cm^{-1} were assigned to N-H stretching vibration modes of the coordinated NH_3 [54,55]. The bands at 1198 and 1599 cm^{-1} were attributed to coordinated NH_3 linked to Lewis acid sites (NH_3-L) [34,56], and the bands at 1440 and 1689 cm^{-1} were assigned to asymmetric and symmetric bending vibrations of NH_4^+ bounded to Brønsted acid sites (NH_4^+-B) [15,40,50]. The band at 1258 cm^{-1} was assigned to the deformation vibration of NH_3 bonded to Lewis acid [57].

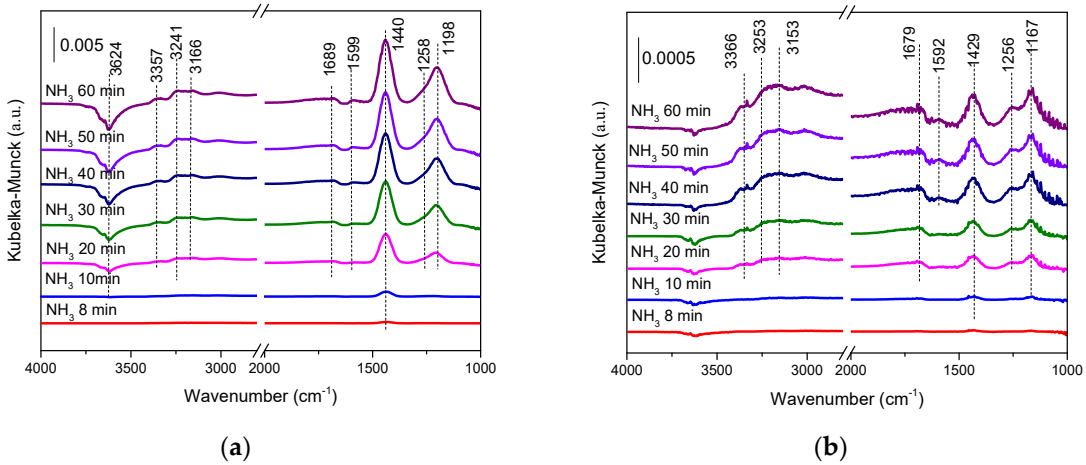

Figure 8. The in situ diffuse reflectance infrared Fourier transform (DRIFT) of NH_3 adsorption over (**a**) the SbCeZr and (**b**) the SbCe catalysts at 200 °C.

NH_4^+-B species (1440 cm^{-1}) appeared after exposing in NH_3 for 8 min over SbCeZr as shown in Figure 8a, and the adsorbed band turned intensive with the consumption of surface hydroxyl groups (3624 cm^{-1}). However, the appearance of NH_3-L species (1198 cm^{-1}) lagged behind. Unlike SbCeZr, NH_4^+-B species (1429, 1679 cm^{-1}) and NH_3-L species (1167, 1256 cm^{-1}) were observed synchronously over SbCe (Figure 8b). Compared with SbCe, an obvious blue shift of NH_3 adsorption on acid sites was found over SbCeZr, presenting the strong NH_3 adsorption on SbCeZr. After exposure in NH_3 for 60 min, the difference in the distribution of NH_4^+-B and NH_3-L species was found. It should be recalled that a great discrepancy was noticed for the bands of NH_4^+-B and NH_3-L species in two samples. By calculating the band intensity of NH_3 adsorption, a high proportion of NH_4^+-B species was found on SbCeZr, while the proportions of NH_4^+-B and NH_3-L species on SbCe were similar. The presence of abundant Brønsted and Lewis acid sites on the SbCeZr catalyst should be responsible for the improvement in SCR activities over a wide temperature range [58].

2.3.2. Adsorption of NH_3 Followed by Introduction of NO + O_2

The spectra of introducing NO + O_2 into the catalysts after NH_3 adsorption as a function of time were recorded and are shown in Figure 9. The decrease of NH_4^+-B and NH_3-L species on SbCeZr with the introduction of NO + O_2 presented the reaction between NO_x and adsorbed NH_3 species (Figure 9a). The intensities of the bands ascribed to NH_3-L and NH_4^+-B species were reduced after NH_3 adsorption, showing that these surface species were able to react with the mixture of NO and O_2 at 200 °C. A deeper insight into the reduction of band intensity with the reaction time over the catalysts was essential. The further investigation on the consumption rate of NH_3-L and NH_4^+-B species showed the slightly faster disappearance of NH_3-L species than NH_4^+-B species in the reaction. Extending the exposure time led to the appearance of nitrate species, such as bridged nitrate (1605 and 1247 cm^{-1}) [59], bidentate nitrate (1579, 1559, and 1516 cm^{-1}) [55], and monodentate nitrate (1541 cm^{-1}) [60]. The recovery of the negative broad band of surface hydroxyl groups (3441 cm^{-1}) was attributed to the formation of water, which further confirmed the occurrence of the reaction.

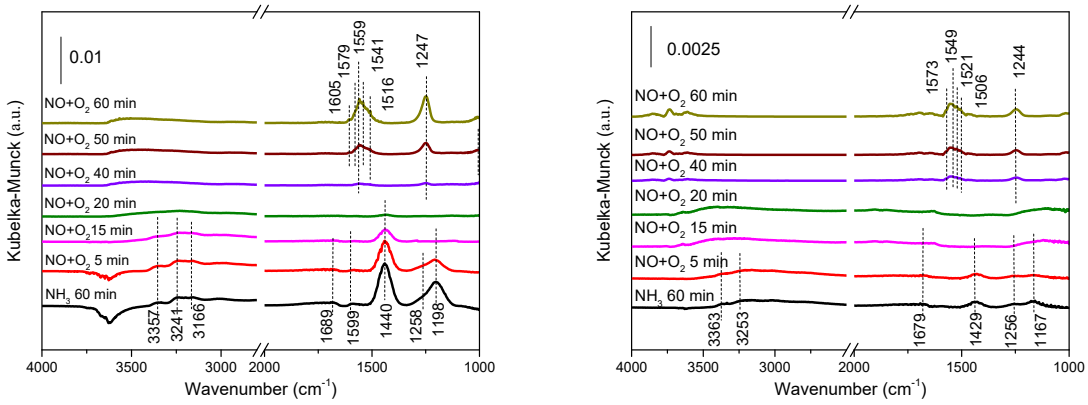

(**a**) (**b**)

Figure 9. The in situ DRIFT of NO + O_2 reacting with preadsorbed NH_3 species over (**a**) the SbCeZr and (**b**) the SbCe catalysts at 200 °C.

As shown in Figure 9b, the phenomenon that occurred on SbCe was similar to that on SbCeZr, i.e., the appearance of nitrate species at the expense of the disappearance of adsorbed NH_3. The disappearance of NH_3-L species confirmed that NH_3-L species could be involved in the reaction, and NH_3-L species were slightly active compared with NH_4^+-B species. The adsorbed NH_3 on the catalyst surface reacted with NO/NO_2 in the gas phase, following the Eley-Rideal (E-R) mechanism.

2.3.3. Co-Adsorption of NO + O_2

The adsorption of NO + O_2 was investigated by in situ DRIFT. As shown in Figure 10a, bridged nitrate (1245, 1606 cm^{-1}), bidentate nitrate (1579, 1559, 1519 cm^{-1}), and monodentate nitrate (1539 cm^{-1}) were formed on SbCeZr after exposure to NO + O_2 for 30 min. The NH_3 adsorption rate was much faster than the NO_x^- generation rate. With the exposure time prolonged, the bands of nitrate intensified accordingly. Bridged nitrate seemed dominant in all the kinds of nitrates. In the case of SbCe (Figure 10b), rather weak bands of nitrates were observed after the exposure to the same feed gas for the same time, and the adsorption intensity of bridged nitrate was rather weaker than that of the monodentate and bidentate nitrates. It could be seen that Sb interacted with different metals (Ce or CeZr), resulting in the difference in the NO_3^- species distribution on the catalyst surface.

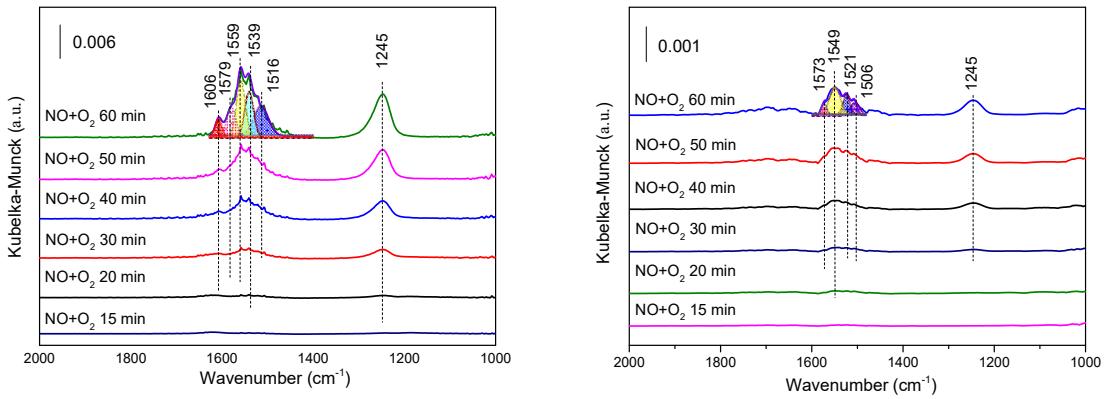

(**a**) (**b**)

Figure 10. The in situ DRIFT of NO + O_2 co-adsorption over (**a**) the SbCeZr and (**b**) the SbCe catalysts at 200 °C.

2.3.4. Adsorption of NO + O_2 Followed by Introduction of NH_3

Compared with the results of NO + O_2 reacting with preadsorbed NH_3 (Figure 9), the effects of adding NH_3 to preadsorbed NO + O_2 (Figure 11) on activity were not so obvious. It is worth mentioning that a new band linked to NH_4^+-B species (1440 cm^{-1}) gradually formed over SbCeZr as the exposure time increased. However, the bands linked to NH_3-L (1599 and 1198 cm^{-1}) were not detected. Therefore, the formed nitrate species had detrimental effects on NH_3 adsorption on Lewis sites, but negligent effects on NH_3 adsorption on Brønsted acid sites.

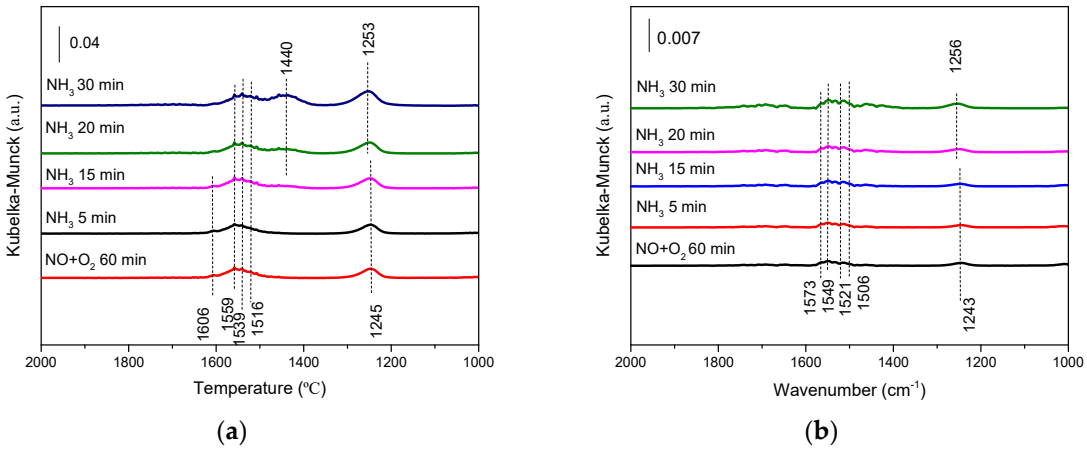

(**a**) (**b**)

Figure 11. The in situ DRIFT of NH_3 reacting with preadsorbed NO + O_2 over (**a**) the SbCeZr and (**b**) the SbCe catalysts at 200 °C.

On the contrary, there were no bands related to NH_3 adsorption over SbCe even after prolonging the exposure time up to 30 min. The phenomena illustrated that the formed nitrate species significantly inhibited NH_3 adsorption. Combined with the results of Figure 11, this indicated that NH_3 adsorption and NO_x oxidation could be competitive on SbCe, but not on SbCeZr.

2.4. Discussion

NO_x conversions over CeO_2 and SbO_x were very low, but it increased significantly when they were combined together. Compared with CeO_2, the reason for the improvement of catalytic activity over $SbCeO_x$ was due to alleviating nitrate adsorption and leaving more active sites for NH_3 adsorption and activation [40]. Considering the competitive adsorption between NH_3 and nitrate species, we prepared SbCeZr and investigated it for NH_3-SCR performance. SbCeZr outperformed SbCe not only in activity and stability but also in SO_2 and water tolerance. SbCeZr exhibited high activity with NO_x conversion over 80% in the temperature range of 202–422 °C. The introduction of H_2O and SO_2 had little influence on the activity of SbCeZr, but an adverse effect on the catalytic activity of SbCe was found.

The presence of Zr influenced the distribution of Sb on the surface or bulk. According to ICP-AES and XPS results (Table 1), the surface amount of Sb on SbCe was much higher than that on SbCeZr, displaying the enrichment of Sb on the SbCe surface. However, H_2-TPR indicated the strong interaction between SbO_x and CeO_2. Unlike SbCe, the presence of Zr made the distribution of Sb, Ce, and Zr uniform and weakened the interaction between SbO_x and CeO_2. The weakened interaction also brought about abundant Sb^{5+} species on the catalyst surface (Table 1) and the lower onset reduction temperature of active oxygen (Figure 5). Furthermore, the generation of NO_2 during NO-TPD (Figure 6) also illustrated the enhancement in reducibility, which facilitated the "fast SCR" reaction during NH_3-SCR [32].

The adsorption of NH_3 on the catalyst surface was considered as the initial step of the NH_3-SCR reaction [15], so NH_3 adsorption played an important role during NO_x removal. Compared with SbCe, NH_3 adsorption was enhanced on SbCeZr, which was attributed to the increase of Brønsted and Lewis

acid amounts (Figure 7). The acid distribution on the catalysts was different. The amount of Brønsted acid was higher than the amount of Lewis acid on SbCeZr, whereas the amount of Brønsted acid was similar to that of Lewis acid on SbCe. Meanwhile, in situ DRIFT experiments of NH_3 adsorption also confirmed the strong adsorption of NH_3 and the faster adsorption rate on SbCeZr (Figure 8). The reaction rate of NO_x with NH_3 adsorbed on Lewis acid was slightly faster than that with NH_4^+ adsorbed on Brønsted acid (Figure 9) (E-R mechanism).

It is worth mentioning that the formed nitrates had negligible effects on the adsorption of NH_3 over SbCeZr; however, detrimental impacts were found over SbCe. It meant that NO oxidation and NH_3 adsorption were both around Ce^{n+} sites, so there was competition between them. Amorphous ZrO_2 possessed abundant hydroxyl [61], which showed obvious acidity properties. Then, the strong withdrawing effects of SbO_x further increased the acid amount and strength of ZrO_2, which was confirmed by the high NH_3 desorption amount (Figure 7). Therefore, the separation of active sites alleviated the competition effects between NO oxidation and NH_3 adsorption, thus promoting NO_x removal.

Given the above discussion, it was shown that the strong acid and weak reducibility of SbZr made it less active in NH_3-SCR. However, a strengthened interaction was found between SbO_x and CeO_2, favoring NO_x removal. Unfortunately, the competition between NO oxidation and NH_3 adsorption on the same active sites still needed to be alleviated to improve its thermostability and activity in the presence of H_2O and SO_2. In the presence of ZrO_2, NH_3 adsorption and NO oxidation on different active sites widened the operation window.

3. Materials and Methods

3.1. Catalyst Preparation

The SbCe, SbCeZr, and SbZr catalysts, where the molar ratio of Sb/Ce and Zr/Ce was 1.0, were prepared by the citric acid method. First, $Sb(CH_3COO)_3$ was dissolved in a solution of citric acid, then $Zr(NO_3)_4$ and $Ce(NO_3)_4$ were added. The molar ratio of citric acid to total metal components (the sum of Ce, Zr, and Sb) was 1.5. Then, the resultant mixture was stirred at 80 °C in a water bath until forming a gel. The gel was dried at 110 °C for 12 h to form a porous, foamlike solid. Finally, the precursor was calcined at 500 °C for 3 h in a muffle furnace (SX2, Shanghai Pudong Rong-Feng Scientific Instrument Co. Ltd., Shanghai, China). After calcining, the sample was crushed and sieved to 40–60 mesh prior to evaluation. CeO_2, SbO_x, and ZrO_2 were also prepared by the same method.

3.2. Catalytic Activity Testing

The catalytic activities of the catalysts for the selective catalytic reduction of NO_x with NH_3 in excess oxygen were conducted at atmospheric pressure in a fixed-bed continuous flow quartz reactor. In the evaluation, a 200 mg portion of catalyst (40–60 mesh) was applied, and the feed gas contained 500 ppm NO, 500 ppm NH_3, 5% O_2, 5% H_2O (when used), 100 ppm SO_2 (when used), and Ar balance. The total flow was 300 mL/min and the gas hourly space velocity (GHSV) was about 150,000 h^{-1}. A Thermo Fisher NO-NO_x-chemiluminescence analyzer (Waltham, MA, USA) was used to detect the concentration of NO and NO_2 before and after the reaction. The catalyst bed was heated at 2 °C/min, held for 45 min every 50 °C, and then the concentration of NO_x was measured. NO_x conversion was calculated using the following equation:

$$NO_x \text{ conversion} = \frac{[NO_x]_{in} - [NO_x]_{out}}{[NO_x]_{in}} \times 100\% \quad (1)$$

where $[NO_x]_{in}$ and $[NO_x]_{out}$ represented the inlet and outlet concentrations of NO_x, respectively.

3.3. Catalyst Characterization

The N_2 adsorption–desorption isotherms were measured on a Quantachrome NOVA1200 analyzer (Norcross, GA, USA) at −196 °C to obtain the surface area of the catalysts. Before measurement, the catalyst was degassed at 180 °C until it reached a stable vacuum of approximately 5 mTorr. After calculating the desorption data using the Brunauer–Emmett–Teller (BET) method, the specific surface area was obtained. The X-ray diffraction (XRD) patterns were carried out on a Bruker/D8 diffractometer (Karlsruhe, Germany) with Cu Kα radiation (λ = 0.154 nm). The X-ray photoelectron spectroscopy (XPS) spectra were obtained using a Thermo Scientific ESCALAB 250 spectrometer analyzer (Waltham, MA, USA), using a monochromatized Al-Kα source (1486.6 eV), and the binding energy of adventitious carbon (284.6 eV) was taken as a reference.

The temperature-programmed reduction of H_2 (H_2-TPR) and the temperature-programmed desorption of NH_3 (NH_3-TPD) were performed on a PX200 apparatus (Tianjin Pengxiang Technology Co. Ltd., Tianjin, China) with a thermal conductivity detector (TCD). For the H_2-TPR experiment, a 100 mg portion of catalyst was pretreated in N_2 at 300 °C for 30 min, then cooled down to 30 °C. Finally, the catalyst was heated from 30 °C to 800 °C at a rate of 10 °C/min in 5% H_2/Ar (40 mL/min). For the NH_3-TPD, a 100 mg portion of catalyst was pretreated at 500 °C under a flow of Ar (50 mL/min) for 1 h, and the pretreated catalyst was exposed to a flow of 10% NH_3/Ar (40 mL/min) for 1 h at 100 °C. Then, the sample was flushed by Ar (50 mL/min) for 1 h and heated from 100 °C to 500 °C at 10 °C/min.

The temperature-programmed desorption of NO (NO-TPD) experiments were conducted on custom-made equipment with a NO_x analyzer. Before testing, a 200 mg portion of catalyst was pretreated at 500 °C under a flow of Ar (300 mL/min) for 1 h; after cooling to room temperature, the pretreated catalyst adsorbed NO with a flow of 500 ppm NO/Ar (300 mL/min) for 1 h. The catalyst was flushed by Ar (300 mL/min) for 1 h and then heated from room temperature to 500 °C at 10 °C/min.

In situ DRIFT spectra were collected using an FTIR spectrometer (Thermo Nicolet 6700, Waltham, MA, USA) with an MCT detector cooled by liquid nitrogen. Before each experiment, the catalyst was pretreated at 300 °C for 1 h in Ar (50 mL/min). After the temperature cooling to 200 °C, 1000 ppm NH_3/Ar was introduced into the IR cell and the background was subtracted from the sample spectra. After adsorption saturation, 1000 ppm NO + 5% O_2/Ar was introduced to replace NH_3 at 200 °C. The experiment of NO + O_2 adsorption and reaction with NH_3 was carried out following a similar process. First, the catalyst was pretreated at 300 °C for 1 h in Ar (50 mL/min), then 1000 ppm NO + 5% O_2/Ar adsorption was carried out at 200 °C, and finally 1000 ppm NH_3/Ar was introduced to replace NO + O_2.

4. Conclusions

Sb-containing metal oxides (SbZr, SbCe, SbCeZr) were prepared by citric acid method and investigated for NH_3-SCR. SbCeZr exhibited the higher performance in NH_3-SCR than SbCe and SbZr, and NO_x could be removed with 80% conversion in the temperature range of 202–422 °C. SbCeZr owned excellent activity even in the presence of water and SO_2, and the thermostability was improved compared with SbCe. Hence, SbCeZr seemed to be a good candidate for the practical application in deNO_x. The presence of Sb in the metal oxides led to the difference in acid distribution and redox property, which was closely related to the NH_3 adsorption and NO oxidation. Brønsted acid and Lewis acid distributed evenly on SbCe, while Brønsted acid dominated on SbCeZr. Although high amounts of acid were on SbZr, poor redox led to its negligent performance in NH_3-SCR. The enhancement in redox ability promoted the generation of nitrates on SbCe. However, the competition between NO oxidation and NH_3 adsorption on the same active sites limited its application. In the presence of ZrO_2, the interaction between Sb and Ce was weakened, which further increased the acid amount and redox property. The form of "dual active sites" favored the NH_3 adsorption and nitrate generation.

Author Contributions: Conceptualization, Q.X. and L.W.; methodology, Q.X., D.L. and C.W.; validation, L.W. and Y.G. (Yun Guo); formal analysis, Q.X., L.W., Q.K. and M.N.H.; investigation, D.L., Q.K. and M.N.H.; resources, W.Z., Y.G. (Yun Guo) and Y.G. (Yanglong Guo); data curation, Q.X., Q.K. and L.W.; writing—original draft preparation, Q.X. and L.W.; writing—review and editing, Q.X., L.W. and W.Z.; project administration, Y.G. (Yanglong Guo); funding acquisition, Y.G. (Yun Guo) and Y.G. (Yanglong Guo). All authors have read and agreed to the published version of the manuscript.

Funding: This project was supported financially by the National Key Research and Development Program of China (2016YFC0204300) and the National Natural Science Foundation of China (21976057 and 21922602), as well as the "Shanghai Science and Technology Innovation Plan" Program (19DZ1208000), and Fundamental Research Funds for the Central Universities.

Conflicts of Interest: The authors declare no conflict of interest.

References

1. Irfan, M.F.; Goo, J.H.; Kim, S.D. Co_3O_4 based catalysts for NO oxidation and NOx reduction in fast SCR process. *Appl. Catal. B Environ.* **2008**, *78*, 267–274. [CrossRef]
2. Fu, M.; Li, C.; Lu, P.; Qu, L.; Zhang, M.; Zhou, Y.; Yu, M.; Fang, Y. A review on selective catalytic reduction of NOx by supported catalysts at 100–300 °C—Catalysts, mechanism, kinetics. *Catal. Sci. Technol.* **2014**, *4*, 14–25. [CrossRef]
3. Xu, Q.; Fang, Z.L.; Chen, Y.Y.; Guo, Y.L.; Guo, Y.; Wang, L.; Wang, Y.S.; Zhang, J.S.; Zhan, W.C. Titania–Samarium–Manganese Composite Oxide for the Low-Temperature Selective Catalytic Reduction of NO with NH_3. *Environ. Sci. Technol.* **2020**, *54*, 2530–2538. [CrossRef]
4. Zhan, W.C.; Guo, Y.; Gong, X.Q.; Guo, Y.L.; Wang, Y.Q.; Lu, G.Z. Current status and perspectives of rare earth catalytic materials and catalysis. *Chin. J. Catal.* **2014**, *35*, 1238–1250. [CrossRef]
5. Peng, Y.; Wang, D.; Li, B.; Wang, C.; Li, J.; Crittenden, J.; Hao, J. Impacts of Pb and SO_2 Poisoning on CeO_2–WO_3/TiO_2–SiO_2 SCR Catalyst. *Environ. Sci. Technol.* **2017**, *51*, 11943–11949. [CrossRef]
6. Xu, T.; Wu, X.; Gao, Y.; Lin, Q.; Hu, J.; Wang, D. Comparative study on sulfur poisoning of V_2O_5-Sb_2O_3/TiO_2 and V_2O_5-WO_3/TiO_2 monolithic catalysts for low-temperature NH_3-SCR. *Catal. Commun.* **2017**, *93*, 33–36. [CrossRef]
7. Kwon, D.W.; Hong, S.C. Enhancement of performance and sulfur resistance of ceria-doped V/Sb/Ti by sulfation for selective catalytic reduction of NOx with ammonia. *RSC Adv.* **2016**, *6*, 1169–1181. [CrossRef]
8. Xu, L.; Wang, C.; Chang, H.; Wu, Q.; Zhang, T.; Li, J. New Insight into SO_2 Poisoning and Regeneration of CeO_2–WO_3/TiO_2 and V_2O_5–WO_3/TiO_2 Catalysts for Low-Temperature NH_3–SCR. *Environ. Sci. Technol.* **2018**, *52*, 7064–7071. [CrossRef]
9. Zhang, H.; Sun, K.; Feng, Z.; Ying, P.; Li, C. Studies on the SbOx species of SbOx/SiO_2 catalysts for methane-selective oxidation to formaldehyde. *Appl. Catal. A Gen.* **2006**, *305*, 110–119. [CrossRef]
10. Qu, R.; Gao, X.; Cen, K.; Li, J. Relationship between structure and performance of a novel cerium-niobium binary oxide catalyst for selective catalytic reduction of NO with NH_3. *Appl. Catal. B Environ.* **2013**, *142*, 290–297. [CrossRef]
11. Topsøe, N.Y. Mechanism of the selective catalytic reduction of nitric oxide by ammonia elucidated by in situ on-line Fourier transform infrared spectroscopy. *Science* **1994**, *265*, 1217–1219. [CrossRef] [PubMed]
12. Zhang, T.; Qu, R.; Su, W.; Li, J. A novel Ce–Ta mixed oxide catalyst for the selective catalytic reduction of NOx with NH_3. *Appl. Catal. B Environ.* **2015**, *176*, 338–346. [CrossRef]
13. Guo, R.; Sun, X.; Liu, J.; Pan, W.; Li, M.; Sun, P.; Liu, S. Enhancement of the NH_3-SCR catalytic activity of $MnTiO_x$ catalyst by the introduction of Sb. *Appl. Catal. A Gen.* **2018**, *558*, 1–8. [CrossRef]
14. Shi, R.H.; Lin, X.Y.; Zheng, Z.G.; Feng, R.; Liu, Y.M.; Ni, L.F.; Yuan, B.H. Selective catalytic reduction of NOx with NH_3 over Sb modified CeZrOx catalyst. *React. Kinet. Mech. Cat.* **2018**, *124*, 217–227. [CrossRef]
15. Liu, J.; Li, G.; Zhang, Y.; Liu, X.; Wang, Y.; Li, Y. Novel Ce-W-Sb mixed oxide catalyst for selective catalytic reduction of NOx with NH_3. *Appl. Surf. Sci.* **2017**, *401*, 7–16. [CrossRef]
16. Danh, H.T.; Kumar, P.A.; Jeong, Y.E.; Ha, H.P. Enhanced NH_3-SCR activity of Sb-V/CeO_2–TiO_2 catalyst at low temperatures by synthesis modification. *Res. Chem. Intermed.* **2016**, *42*, 155–169. [CrossRef]
17. Du, X.; Gao, X.; Fu, Y.; Gao, F.; Luo, Z.; Cen, K. The co-effect of Sb and Nb on the SCR performance of the V_2O_5/TiO_2 catalyst. *J. Colloid Interface Sci.* **2012**, *368*, 406–412. [CrossRef]

18. Phil, H.H.; Reddy, M.P.; Kumar, P.A.; Ju, L.K.; Hyo, J.S. SO_2 resistant antimony promoted V_2O_5/TiO_2 catalyst for NH_3-SCR of NOx at low temperatures. *Appl. Catal. B Environ.* **2008**, *78*, 301–308. [CrossRef]
19. Kim, J.; Lee, S.; Kwon, D.W.; Lee, K.Y.; Ha, H.P. SO_3^{2-}/SO_4^{2-} functionalization-tailorable catalytic surface features of Sb-promoted $Cu_3V_2O_8$ on TiO_2 for selective catalytic reduction of NO_X with NH_3. *Appl. Catal. A Gen.* **2019**, *570*, 355–366. [CrossRef]
20. Ding, Y.Q.; Wu, Q.Q.; Li, B.; Guo, Y.L.; Guo, Y.; Wang, Y.S.; Wang, L.; Zhan, W.C. Superior catalytic activity of a Pd catalyst in methane combustion by fine-tuning the phase of ceria-zirconia support. *Appl. Catal. B Environ.* **2020**, *266*, 118631. [CrossRef]
21. Li, Y.; Cheng, H.; Li, D.; Qin, Y.; Xie, Y.; Wang, S. ChemInform Abstract: WO_3/CeO_2—ZrO_2, a Promising Catalyst for Selective Catalytic Reduction (SCR) of NO_x with NH_3 in Diesel Exhaust. *Chem. Commun.* **2008**, *12*, 1470–1472. [CrossRef] [PubMed]
22. Shen, B.; Wang, Y.; Wang, F.; Liu, T. The effect of Ce–Zr on NH_3 -SCR activity over $MnO_x(0.6)/Ce_{0.5}$ $Zr_{0.5}$ O_2 at low temperature. *Chem. Eng. J.* **2014**, *236*, 171–180. [CrossRef]
23. Ning, P.; Song, Z.; Li, H.; Zhang, Q.; Liu, X.; Zhang, J.; Tang, X.; Huang, Z. Selective catalytic reduction of NO with NH_3 over CeO_2–ZrO_2–WO_3 catalysts prepared by different methods. *Appl. Surf. Sci.* **2014**, *236*, 171–180. [CrossRef]
24. Ding, S.; Liu, F.; Shi, X.; Liu, K.; Lian, Z.; Xie, L.; He, H. Significant Promotion Effect of Mo Additive on a Novel Ce-Zr Mixed Oxide Catalyst for the Selective Catalytic Reduction of NOx with NH_3. *ACS Appl. Mater. Interfaces* **2015**, *7*, 9497–9506. [CrossRef]
25. Hu, H.; Zha, K.; Li, H.; Shi, L.; Zhang, D. In situ DRIFTs investigation of the reaction mechanism over MnO_x-$MO_y/Ce_{0.75}Zr_{0.25}O_2$ (M = Fe, Co, Ni, Cu) for the selective catalytic reduction of NO_x with NH_3. *Appl. Surf. Sci.* **2016**, *387*, 921–928. [CrossRef]
26. Peng, Y.; Wang, C.; Li, J. Structure–activity relationship of VO_x/CeO_2 nanorod for NO removal with ammonia. *Appl. Catal. B Environ.* **2014**, *144*, 538–546. [CrossRef]
27. Peng, Y.; Li, J.; Huang, X.; Li, X.; Su, W.; Sun, X.; Wang, D.; Hao, J. Deactivation mechanism of potassium on the V_2O_5/CeO_2 catalysts for SCR reaction: Acidity, reducibility and adsorbed-NOx. *Environ. Sci. Technol.* **2014**, *48*, 4515–4520. [CrossRef]
28. Zhang, L.; Li, L.; Gao, Y.; Yao, X.; Ge, C.; Gao, F.; Deng, Y.; Tang, C.; Dong, L. Getting insight into the influence of SO_2 on TiO_2/CeO_2 for the selective catalytic reduction of NO by NH_3. *Appl. Catal. B Environ.* **2015**, *165*, 589–598. [CrossRef]
29. Xu, H.; Sun, M.; Liu, S.; Li, Y.; Wang, J.; Chen, Y. Effect of the calcination temperature of cerium–zirconium mixed oxides on the structure and catalytic performance of $WO_3/CeZrO_2$ monolithic catalyst for selective catalytic reduction of NO_x with NH_3. *RSC Adv.* **2017**, *7*, 24177–24187. [CrossRef]
30. Chen, Z.; Si, Z.; Cao, L.; Wu, X.; Ran, R.; Weng, D. Decomposition behavior of ammonium nitrate on ceria catalysts and its role in the NH_3-SCR reaction. *Catal. Sci. Technol.* **2017**, *7*, 2531–2541. [CrossRef]
31. Huang, Z.; Zhu, Z.; Liu, Z. Combined effect of H_2O and SO_2 on V_2O_5/AC catalysts for NO reduction with ammonia at lower temperatures. *Appl. Catal. B Environ.* **2002**, *39*, 361–368. [CrossRef]
32. Wang, Z.; Guo, R.; Shi, X.; Pan, W.; Liu, J.; Sun, X.; Liu, S.; Liu, X.; Qin, H. The enhanced performance of Sb-modified Cu/TiO_2 catalyst for selective catalytic reduction of NOx with NH_3. *Appl. Surf. Sci.* **2019**, *475*, 334–341. [CrossRef]
33. Wang, Z.; Huang, Z.P.; Brosnahan, J.T.; Zhang, S.; Guo, Y.L.; Guo, Y.; Wang, L.; Wang, Y.S.; Zhan, W.C. Ru/CeO_2 Catalyst with Optimized CeO_2 Support Morphology and Surface Facets for Propane Combustion. *Environ. Sci. Technol.* **2019**, *53*, 5349–5358. [CrossRef] [PubMed]
34. Ali, S.; Chen, L.; Yuan, F.; Li, R.; Zhang, T.; Bakhtiar, S.H.; Leng, X.; Niu, X.; Zhu, Y. Synergistic effect between copper and cerium on the performance of Cu_x-$Ce_{0.5-x}$-$Zr_{0.5}$ (x = 0.1–0.5) oxides catalysts for selective catalytic reduction of NO with ammonia. *Appl. Catal. B Environ.* **2017**, *210*, 223–234. [CrossRef]
35. Guan, B.; Lin, H.; Zhu, L.; Huang, Z. Selective Catalytic Reduction of NO_x with NH_3 over Mn, Ce Substitution $Ti_{0.9}V_{0.1}O_{2-\delta}$ Nanocomposites Catalysts Prepared by Self-Propagating High-Temperature Synthesis Method. *J. Phys. Chem. C* **2011**, *115*, 12850–12863. [CrossRef]
36. Carja, G.; Kameshima, Y.; Okada, K.; Madhusoodana, C.D. Mn–Ce/ZSM5 as a new superior catalyst for NO reduction with NH_3. *Appl. Catal. B Environ.* **2007**, *73*, 60–64. [CrossRef]
37. Xu, H.; Zhang, Q.; Qiu, C.; Lin, T.; Gong, M.; Chen, Y. Tungsten modified MnO_x–CeO_2/ZrO_2 monolith catalysts for selective catalytic reduction of NO_x with ammonia. *Chem. Eng. Sci.* **2012**, *76*, 120–128. [CrossRef]

38. Liu, Z.; Yi, Y.; Zhang, S.; Zhu, T.; Zhu, J.; Wang, J. Selective catalytic reduction of NO_x with NH_3 over Mn-Ce mixed oxide catalyst at low temperatures. *Catal. Today* **2013**, *216*, 76–81. [CrossRef]
39. Cheng, Y.; Song, W.; Liu, J.; Zheng, H.; Zhao, Z.; Xu, C.; Wei, Y.; Hensen, E. Simultaneous NO_x and Particulate Matter Removal from Diesel Exhaust by Hierarchical Fe-Doped Ce–Zr Oxide. *ACS Catal.* **2017**, *7*, 3883–3892. [CrossRef]
40. Liu, Z.; Liu, H.; Zeng, H.; Xu, Q. A novel Ce-Sb binary oxide catalyst for the selective catalytic reduction of NOx with NH_3. *Catal. Sci. Technol.* **2016**, *6*, 8063–8071. [CrossRef]
41. Adamowska, M.; Krzton, A.; Najbar, M.; Costa, P.D. DRIFT study of the interaction of NO and O_2 with the surface of $Ce_{0.62}Zr_{0.38}O_2$ as deNO_x catalyst. *Catal. Today* **2008**, *137*, 288–291. [CrossRef]
42. Meng, D.; Zhan, W.; Guo, Y.; Guo, Y.; Wang, Y.; Wang, L.; Lu, G. A highly effective catalyst of Sm-Mn mixed oxide for the selective catalytic reduction of NO_x with ammonia: Effect of the calcination temperature. *J. Mol. Catal. A Chem.* **2016**, *420*, 272–281. [CrossRef]
43. Shao, C.; Liu, X.; Meng, D.; Xu, Q.; Guo, Y.; Guo, Y.; Zhan, W.; Wang, L.; Lu, G. Catalytic performance of Co–Fe mixed oxide for NH_3-SCR reaction and the promotional role of cobalt. *RSC Adv.* **2016**, *6*, 66169–66179. [CrossRef]
44. Liu, F.; Shan, W.; Lian, Z.; Xie, L.; Yang, W.; He, H. Novel MnWOx catalyst with remarkable performance for low temperature NH_3-SCR of NOx. *Catal. Sci. Technol.* **2013**, *3*, 2699–2707. [CrossRef]
45. Chen, L.; Si, Z.; Wu, X.; Weng, D. DRIFT Study of CuO–CeO_2–TiO_2 Mixed Oxides for NOx Reduction with NH_3 at Low Temperatures. *ACS Appl. Mater. Interfaces* **2014**, *6*, 8134–8145. [CrossRef] [PubMed]
46. Onfroy, T.; Clet, G.; Houalla, M. Correlations between Acidity, Surface Structure, and Catalytic Activity of Niobium Oxide Supported on Zirconia. *J. Phys. Chem. B* **2005**, *109*, 14588–14594. [CrossRef] [PubMed]
47. Ma, Z.; Wu, X.; Si, Z.; Weng, D.; Ma, J.; Xu, T. Impacts of niobia loading on active sites and surface acidity in NbO_x/CeO_2–ZrO_2 NH_3–SCR catalysts. *Appl. Catal. B Environ.* **2015**, *179*, 380–394. [CrossRef]
48. Zuo, J.; Chen, Z.; Wang, F.; Yu, Y.; Wang, L.; Li, X. Low-Temperature Selective Catalytic Reduction of NOx with NH_3 over Novel Mn–Zr Mixed Oxide Catalysts. *Ind. Eng. Chem. Res.* **2014**, *53*, 2647–2655. [CrossRef]
49. Roy, S.; Hegde, M.S.; Madras, G. Catalysis for NOx abatement. *Appl. Eng.* **2009**, *86*, 2283–2297. [CrossRef]
50. Lee, K.J.; Kumar, P.A.; Maqbool, M.S.; Rao, K.N.; Song, K.H.; Ha, H.P. Ceria added Sb-V_2O_5/TiO_2 catalysts for low temperature NH_3 SCR: Physico-chemical properties and catalytic activity. *Appl. Catal. B Environ.* **2013**, *142–143*, 705–717. [CrossRef]
51. Li, L.; Zhang, L.; Ma, K.; Zou, W.; Cao, Y.; Xiong, Y.; Tang, C.; Dong, L. Ultra-low loading of copper modified TiO_2/CeO_2 catalysts for low-temperature selective catalytic reduction of NO by NH_3. *Appl. Catal. B Environ.* **2017**, *207*, 366–375. [CrossRef]
52. Shen, Y.; Zhu, S.; Qiu, T.; Shen, S. A novel catalyst of CeO_2/Al_2O_3 for selective catalytic reduction of NO by NH_3. *Catal. Commun.* **2009**, *11*, 20–23. [CrossRef]
53. Hu, W.; Zhang, Y.; Liu, S.; Zheng, C.; Gao, X.; Nova, I.; Tronconi, E. Improvement in activity and alkali resistance of a novel V-Ce$(SO_4)_2$/Ti catalyst for selective catalytic reduction of NO with NH_3. *Appl. Catal. B Environ.* **2017**, *206*, 449–460. [CrossRef]
54. Nam, K.B.; Kwon, D.W.; Hong, S.C. DRIFT study on promotion effects of tungsten-modified Mn/Ce/Ti catalysts for the SCR reaction at low-temperature. *Appl. Catal. A Gen.* **2017**, *542*, 55–62. [CrossRef]
55. Kumar, P.A.; Jeong, Y.E.; Ha, H.P. Low temperature NH_3 -SCR activity enhancement of antimony promoted vanadia-ceria catalyst. *Catal. Today* **2017**, *293–294*, 61–72. [CrossRef]
56. Yang, N.; Guo, R.; Pan, W.; Chen, Q.; Wang, Q.; Lu, C. The promotion effect of Sb on the Na resistance of Mn/TiO_2 catalyst for selective catalytic reduction of NO with NH_3. *Fuel* **2016**, *169*, 87–92. [CrossRef]
57. Matrails, H.K.; Ciardelli, M.; Ruwet, M.; Grange, P. Vanadia Catalysts Supported on Mixed TiO_2-Al_2O_3 Supports: Effect of Composition on the Structure and Acidity. *J. Catal.* **1995**, *157*, 368–379. [CrossRef]
58. Amiridis, M.D.; Duevel, R.V.; Wachs, I.E. The effect of metal oxide additives on the activity of V_2O_5/TiO_2 catalysts for the selective catalytic reduction of nitric oxide by ammonia. *Appl. Catal. B Environ.* **1999**, *20*, 111–122. [CrossRef]
59. Liu, Y.; Gu, T.; Weng, X.; Wang, Y.; Wu, Z.; Wang, H. DRIFT Studies on the Selectivity Promotion Mechanism of Ca-Modified Ce-Mn/TiO_2 Catalysts for Low-Temperature NO Reduction with NH_3. *J. Phys. Chem. C* **2012**, *116*, 16582–16592. [CrossRef]

60. Jiang, B.; Li, Z.; Lee, S. Mechanism study of the promotional effect of O_2 on low-temperature SCR reaction on Fe–Mn/TiO_2 by DRIFT. *Chem. Eng. J.* **2013**, *225*, 52–58. [CrossRef]
61. Ma, Z.; Xu, R.; Yang, C.; Wei, W.; Li, W.; Sun, Y. Preparation and Surface Properties of Different Zirconia Polymorphs. *Acta Phys.-Chim. Sin.* **2004**, *20*, 1221–1225.